Available online at www.sciencedirect.com
ScienceDirect
Journal of Sound and Vibration 318 (2008) 227–246
JOURNAL OF SOUND AND VIBRATION
www.elsevier.com/locate/jsvi

Out-of-plane free vibrations of curved beams with variable curvature

Byoung Koo Lee[a,*], Sang Jin Oh[b], Jeong Man Mo[c], Tae Eun Lee[a]

[a]Department of Civil and Environmental Engineering, Wonkwang University, Iksan-si, Jeollabuk-do 570-749, Republic of Korea
[b]Department of Civil Engineering, Namdo Provincial College, Damyang-eup, Jeollanam-do 517-802, Republic of Korea
[c]Department of Civil Engineering, Jeonju Life Science Highschool, Jeonju-si, Jeollabuk-do 561-123, Republic of Korea

Received 22 October 2007; received in revised form 29 February 2008; accepted 9 April 2008
Handling Editor: L.G. Tham
Available online 3 June 2008

Abstract

The differential equations governing out-of-plane free vibrations of the elastic, horizontally curved beams with variable curvature are derived and solved numerically to obtain natural frequencies and mode shapes for parabolic, sinusoidal and elliptic beams with hinged–hinged, hinged–clamped, and clamped–clamped end constraints, in which the effects of the rotatory and torsional inertias and shear deformation are included. Experimental measures of frequencies for several laboratory-scale parabolic models serve to validate the theoretical results.

1. Introduction

Since horizontally curved beams are basic structural components, studies on the free vibrations of linearly elastic curved beams of various shapes have been reported for more than three decades. Accurate predictions of the natural frequencies for the free vibrations are important in the design of structures, especially when dynamic loads are subjected. The dynamic behavior of structures including curved beams may be affected by various parameters such as the beam shape, end constraint, inertia force, shear deformation, variable curvature, cross-sectional shape, etc.

Following references and their citations included the governing equations and the significances of the free, out-of-plane vibrations of curved beams. Briefly, these works included studies of beams with prediction of the exact natural frequency by Gupter and Howson [1], Howson et al. [2], and Howson and Jemah [3]; and studies showing the effects of transverse shear, rotatory inertia on natural frequencies by Wang and Guilbert [4], Issa et al. [5], and Kang et al. [6]. Also, natural frequencies of beams with the variable curvature had been computed by Wang [7], Takahashi and Suzuki [8] and Scott and Woodhouse [9]; beams with variable cross-section by Gendy and Saleeb [10], Kawakami et al. [11] and Lee et al. [12]; beams with the continuous span by

*Corresponding author. Tel.: +82 63 850 6718; fax: +82 63 857 7204.
E-mail address: bkleest@wku.ac.kr (B.K. Lee).

0022-460X/$ - see front matter
doi:10.1016/j.jsv.2008.04.015

Wang et al. [13], Snyder and Wilson [14] and Piovan et al. [15]; and beams with the elastic foundation by Wang and Brannen [16], Issa et al. [17], and Lee et al. [18], respectively.

This paper has four main objectives: (1) to present the differential equations for the out-of-plane free vibration of linearly elastic curved beam; (2) to include effect of variable curvature; (3) to include effects of rotatory and torsional inertias and shear deformation; and (4) to present solutions for the various beam shapes, end constraints and beam parameters.

In this study, differential equations governing the out-of-plane free vibrations of linearly elastic curved beam are derived. The effects of variable curvature, both rotatory and torsional inertias, and shear deformation on natural frequencies are included although warping of the cross-section is excluded. Most of all works in the open literature include the effects of variable curvature, rotatory inertia, torsional inertia and shear deformation separately while this study includes all these effects. In order to present the mode shapes of the stress resultants as well as those of the deformations, non-dimensional equations of the stress resultants are formulated. The differential equations are numerically solved to calculate some higher natural frequencies accompanied with the corresponding mode shapes.

The convergence analysis is conducted to obtain the accurate results of numerical solutions. In numerical examples, the parabolic, sinusoidal and elliptic beams with the hinged–hinged, hinged–clamped, and clamped–clamped end constraints are considered. Effects of the rotatory and torsional inertias and shear deformation on natural frequencies are presented. The frequency curves that present the relationships between the natural frequencies and various beam parameters are presented. Typical mode shapes of the stress resultants as well as those of deformations are presented. Experimental methods are described for measuring the free vibration frequencies for the laboratory-scale parabolic beams, which agree well with those predicted by theory.

2. Mathematical model

The geometry of a uniform, symmetric curved beam with variable curvature placed on the horizontal plane (x, y) is defined in Fig. 1. Both ends are either hinged or clamped. Its dashed line is the undeformed shape of the centerline of the cross-section in the static state. The span length, horizontal rise, subtended angle, and shape of the middle surface are l, h, α, and $y = y(x)$, respectively. Its radius of curvature ρ, a function of the coordinate x, has an inclination θ with the radial direction of left end ($x = 0$). The solid line is one of the typical deformed shapes of the so-called mode shapes in the state of free vibration. The positive deformations in the state of free vibration of the vertical deflection, rotation due to the pure bending, shear distortion and twist angle are denoted as v, ψ, β, and ϕ, respectively, at any coordinates (x, y).

A small element of curved beam in the free vibration state shown in Fig. 2 defines positive directions of the three stress resultants and three inertia loadings. Stress resultants are the shear force Q, bending moment M and torsional moment T, and inertia loadings are the transverse inertia force F_v, rotatory inertia couple C_ψ and torsional inertia moment C_ϕ. With the inertia force, inertia couple and torsional inertia moment treated as equivalent static quantities, the three equations for 'dynamic equilibrium' of the element are

$$Q' - \rho F_v = 0, \quad M' - \rho Q + T + \rho C_\psi = 0, \quad M - T' + \rho C_\phi = 0, \tag{1)-(3}$$

where $(') = \mathrm{d}/\mathrm{d}\theta$.

The beam material is assumed to be linear elastic and then, the stress resultants Q, M, and T that relate to the deformations v, ψ, β, and ϕ are given as [19,20]

$$Q = kGA\beta = kGA(\rho^{-1}v' - \psi), \quad M = \rho^{-1}EI(\phi - \psi'), \quad T = \rho^{-1}GJ(\psi + \phi'), \tag{4)-(6}$$

where k is the shape factor of cross-section, G the shear modulus of elasticity and E Young's modulus, A the area, I the second moment of inertia of area, and J the torsion constant of cross-section, respectively. Note that the β variable in Eq. (4) is the shear distortion so that the effect of shear deformation is included in deriving the governing equations.

When the beam is in a state of free vibration, the beam element having mass is subjected to inertia loadings. The beam is assumed to be in harmonic motion, or each coordinate is proportional to sin (ωt), where ω is the

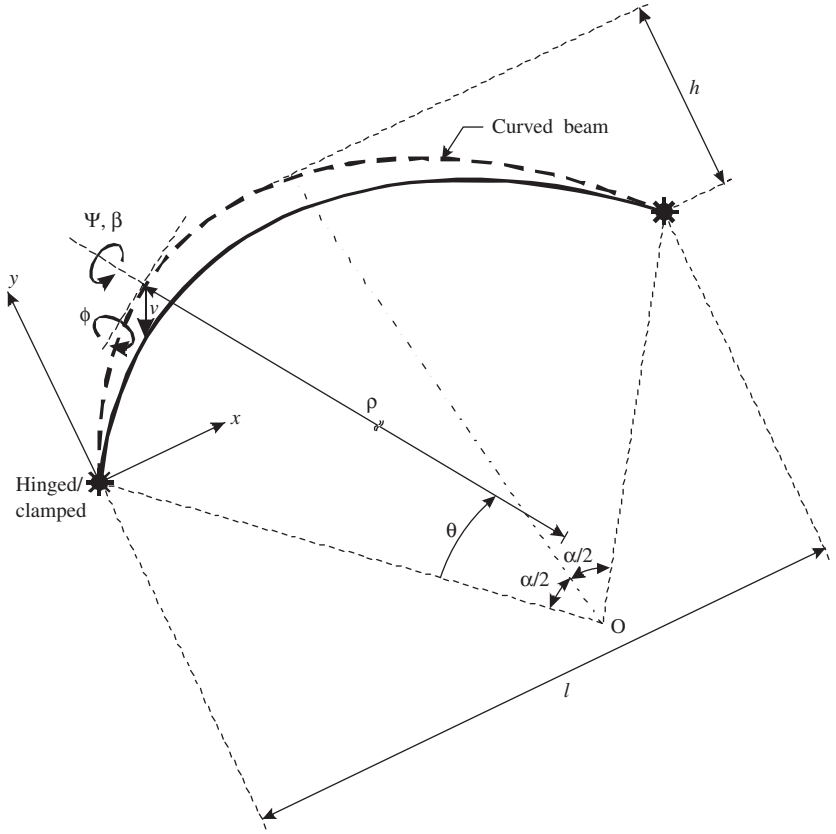

Fig. 1. Curved beam with variable curvature placed on horizontal plane and related variables.

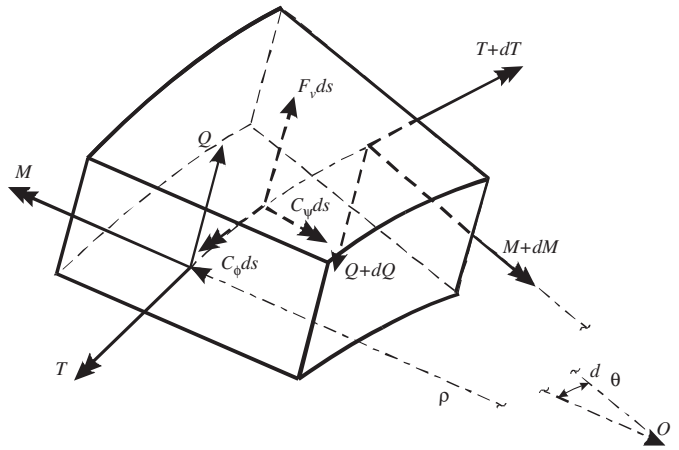

Fig. 2. Loads acting on curved beam element.

angular frequency and t is time. The three inertia loadings are then

$$F_v = -\gamma A\omega^2 v, \quad C_\psi = -\gamma I\omega^2 \psi, \quad C_\phi = -\gamma I_p \omega^2 \phi, \tag{7)-(9}$$

where γ is the mass density of beam material and I_p the polar moment of inertia of area of cross-section. Note that the flexural vibration is caused by the transverse inertia force F_v and the torsional vibration is caused

by the torsional inertia moment C_ϕ. Meanwhile, the rotatory inertia couple C_ψ affects the behavior of the flexural vibration.

When Eqs. (4)–(6) are differentiated once, the results are

$$Q' = kGA[\rho^{-1}(v'' - \rho'\rho^{-1}v') - \psi'],\ M' = EI\rho^{-1}[(\phi' - \psi'') - \rho'\rho^{-1}(\phi - \psi')], \quad (10),(11)$$

$$T' = GJ\rho^{-1}[(\psi' + \phi'') - \rho'\rho^{-1}(\psi + \phi')]. \quad (12)$$

To facilitate the numerical studies and to present the solutions in most general form for this class of problem, the following non-dimensional parameters are defined. The first is the frequency parameter

$$C_i = \omega_i l^2\sqrt{\gamma A/(EI)}, \quad (13)$$

which is written in terms of $\omega = \omega_i$, $i = 1,2,3,\ldots$. The horizontal rise to span length ratio f and two slenderness ratios s and s_p are, respectively,

$$f = h/l, \quad s = l/\sqrt{I/A}, \quad s_p = l/\sqrt{I_p/A}. \quad (14)-(16)$$

Note that in two last equations, the former s is the slenderness ratio respect to I and the latter s_p is one respect to I_p. The torsional rigidity to flexural rigidity ratio and the shear parameter u are, respectively,

$$e = GJ/(EI), \quad u = kG/E. \quad (17),(18)$$

Finally, the coordinates, radius of curvature and vertical deflection are normalized by the span length l:

$$\xi = x/l, \quad \delta = y/l, \quad \zeta = r/l, \quad \eta = v/l. \quad (19)-(22)$$

Differential equations governing out-of-plane free vibrations of the curved beam with variable curvature are derived by using all equations mentioned above. Stress resultants in Eqs. (4)–(6), derivatives of stress resultants in Eqs. (10)–(12) and inertia loadings in Eqs. (7)–(9) are substituted into the three equations of dynamic equilibrium in Eqs. (1)–(3) and the non-dimensional parameters in Eqs. (13)–(22) are used. The results are then

$$\eta'' = \zeta'\zeta^{-1}\eta' - u^{-1}s^{-2}C_i^2\zeta^2\eta + \zeta\psi', \quad (23)$$

$$\psi'' = -us^2\zeta\eta + \zeta'\zeta^{-1}\psi' + (e + us^2\zeta^2 - s^{-2}C_i^2\zeta^2)\psi + (1 + e)\phi' - \zeta'\zeta^{-1}\phi, \quad (24)$$

$$\phi'' = -(1 + e^{-1})\psi' + \zeta'\zeta^{-1}\psi + \zeta'\zeta^{-1}\phi' + e^{-1}(1 - s_p^{-2}C_i^2\zeta^2)\phi. \quad (25)$$

Each end of the beam is either hinged or clamped. The boundary conditions for the hinged end ($\theta = 0$ and α) are

$$\eta = 0, \quad \psi' = 0, \quad \phi = 0, \quad (26)-(28)$$

where Eq. (27) with Eq. (28) assures that the bending moment M in Eq. (5) is zero.

The boundary conditions for the clamped end ($\theta = 0$ and α) are

$$\eta = 0, \quad \psi = 0, \quad \phi = 0 \quad (29)-(31)$$

implying that the deformations v, ψ and ϕ are zero.

For presenting the mode shapes of the stress resultants Q, M, and T as well as those of deformations v, ψ, and ϕ, the following non-dimensional stress resultants are introduced:

$$Q^* = Q/(kGA) = \zeta^{-1}\eta' - \psi, \quad M^* = Ml/(EI) = \zeta^{-1}(\phi - \psi'), \quad (32),(33)$$

$$T^* = Tl/(GJ) = \zeta^{-1}(\psi + \phi'). \quad (34)$$

3. Numerical methods

3.1. Computing method of curvature terms

Coefficients in Eqs. (23)–(25) include two terms of curvature ζ and ζ' at the coordinate θ which are determined when the shape of curved beam is given as the non-dimensional equation of $\delta = \delta(\xi)$. In this section, the determining method of $\delta = \delta(\xi)$ for a given beam shape with the span length l and horizontal rise h, and the computing method of the curvature terms ζ and ζ' of the given beam shape are discussed.

Shown in Fig. 3(a) is a general shape of the beam with l and h placed on the horizontal plane (x, y), from which the equation of beam can be determined as $y = y(x)$. Cast the given beam shape $y = y(x)$ in non-dimensional form using Eqs. (14), (19), and (20). This leads to $\delta = \delta(\xi)$ from which the inclination θ, non-dimensional radius ζ at the coordinate ξ, i.e. at the coordinate x, and subtended angle α, respectively, are determined.

In this study, three kinds of beam shapes of the parabolic, sinusoidal and elliptic beams are selected. The non-dimensional equation $\delta = \delta(\xi)$ of each beam shape is determined as follows [21].

3.1.1. Parabolic beam

The non-dimensional equation $\delta = \delta(\xi)$ for the parabolic beam, depicted in Fig. 3(a), of span length l and horizontal rise h is analytically obtained by using Eqs. (14), (19), and (20), and subsequently, its first derivative $\delta^i = \delta^i(\xi)$ is analytically obtained. The results are

$$\delta = \delta(\xi) = -4f\xi(\xi - 1), \quad \delta^i = \delta^i(\xi) = -4f(2\xi - 1), \tag{35),(36}$$

where $(^i) = \mathrm{d}/\mathrm{d}\xi$.

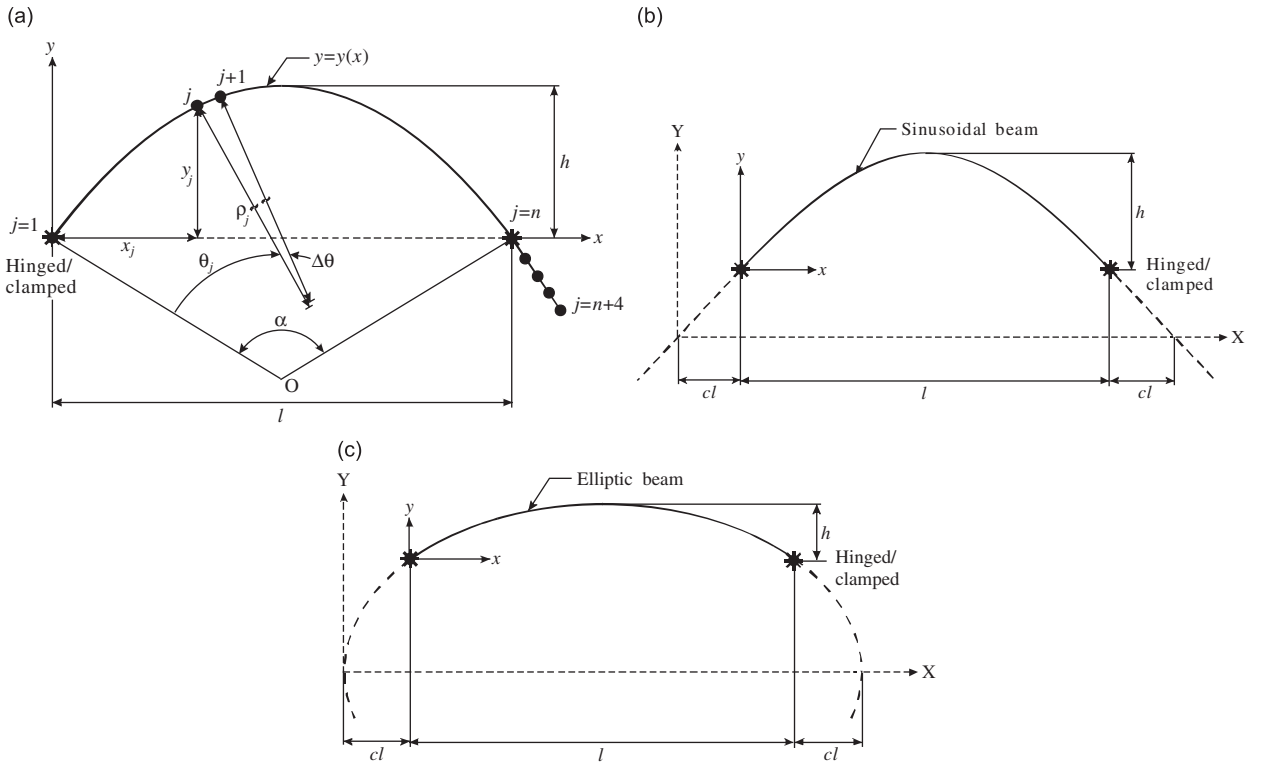

Fig. 3. Beam shapes: (a) general/parabolic, (b) sinusoidal, and (c) elliptic beams.

3.1.2. Sinusoidal beam

Consider now a sinusoidal beam that is a segment of sinusoid, or the solid curve of Fig. 3(b). This beam has span length l and horizontal rise h, and a coordinate system (x, y) originating from the left end. The corresponding half-sine curve, also shown in Fig. 3(b), is composed of this beam segment and the broken line segments extending from each end. This half-sine curve of length $(1+2c)l$ and amplitude H is expressed in terms of the (X, Y) as $Y = H\sin[\pi X/\{(1+2c)l\}]$. The relationship between the two coordinate systems of Fig. 3(b) is $X = cl + x$ and $Y = H - h + y$. When three equations just mentioned are combined together with Eqs. (14), (19), and (20), the general equation for the sinusoidal beam in non-dimensional form can be expressed and also its first derivative is obtained. The results are

$$\delta = \delta(\xi) = a_1 \sin(a_2\xi + a_2 c) + f - a_1, \quad \delta^i = \delta^i(\xi) = a_1 a_2 \cos(a_2\xi + a_2 c), \tag{37),(38}$$

where $a_1 = f/[1-\sin(a_2 c)]$ and $a_2 = \pi/(1+2c)$.

3.1.3. Elliptic beam

The elliptic beam of span length l and horizontal rise h is also defined in non-dimensional form. However, $(1+2c)l$ is the length of the axis of the ellipse as shown in Fig. 3(c). The non-dimensional equation for this beam and its first derivative are

$$\delta = \delta(\xi) = (a_1/a_2)[a_2^2 - (\xi - 1/2)^2]^{1/2} + f - a_1, \tag{39}$$

$$\delta^i = \delta^i(\xi) = -(a_1/a_2)(\xi - 1/2)[a_2^2 - (\xi - 1/2)^2]^{-1/2}, \tag{40}$$

where $a_1 = (a_2 f)/[a_2 - (c + c^2)^{1/2}]$ and $a_2 = 1/2 + c$.

Using the non-dimensional equations δ and δ^i discussed above gives the subtended angle α, the inclination θ and the radius ζ at any coordinate ξ. The results are

$$\alpha = \tan^{-1}[\delta^i(0)] - \tan^{-1}[\delta^i(1)], \quad \theta = \tan^{-1}[\delta^i(0)] - \tan^{-1}[\delta^i(\xi)], \tag{41),(42}$$

$$\zeta = [1 + \{\delta^i(\xi)\}^2]^{3/2}/\delta^{ii}(\xi). \tag{43}$$

Using Eqs. (42) and (43) that are functions of the single coordinate ξ can give the curvature terms ζ and $\zeta'(= d\zeta/d\theta)$ at the inclination θ corresponding to ξ, i.e. at the angular coordinate θ, analytically or numerically. In this study, the numerical method rather than analytical method is chosen. The numerical method computing the curvature terms of ζ and ζ' in Eqs. (23)–(25) are as follows:

(1) Set the beam shape (parabolic or sinusoidal or elliptic), l, h, and c. Recall that the numerical factor c is not available for the parabolic beam.
(2) Form the non-dimensional equation of beam shape, $\delta = \delta(\xi)$, with $f(= h/l)$ and its first derivative $\delta' = \delta'(\xi)$. See Eqs. (35)–(40) in accordance with the selected beam shape.
(3) Compute α using Eq. (41).
(4) Compute $\Delta\theta = \alpha/(n-1)$ where n is the number of dividing elements of the beam arc-length from $\xi = 0$ to 1, i.e. from $x = 0$ to l. See Fig. 3(a).
(5) Compute the angular coordinate $\theta_j = (j-1)\Delta\theta$ at the jth point where $j(= 1,2,3,\ldots,n)$ is the integer number originating from the left end ($\xi = 0$).
(6) Solve the nonlinear equation of Eq. (42), $\theta_j = \tan^{-1}[\delta^i(0)] - \tan^{-1}[\delta^i(\xi_j)]$, and then, obtain the unknown value of ξ_j corresponding to θ_j. Note that the $\delta^i(\xi_j)$ term in Eq. (42) is a function of an unknown variable ξ_j which can be solved by the proper numerical methods such as Regula–Falsi method [22] adopted herein. The function of $\delta^i(\xi_j)$ is defined in Eq. (36) or Eq. (38) or Eq. (40).
(7) Compute derivatives of $\delta_j^{\,i}$ and $\delta_j^{\,ii}$ using the numerical differentiation method. Herein, the forward fourth-order polynomials in Taylor-series method [22] is used, or

$$\delta_j^i = (-25\delta_0 + 48\delta_1 - 36\delta_2 + 16\delta_3 - 3\delta_4)/(12\Delta\xi), \tag{44}$$

$$\delta_j^{ii} = (35\delta_0 - 104\delta_1 + 114\delta_2 - 56\delta_3 + 11\delta_4)/[12(\Delta\xi)^2], \tag{45}$$

where $\delta_0 = \delta(\xi_j)$, $\delta_1 = \delta(\xi_0 + \Delta\xi), \ldots, \delta_4 = \delta(\xi_0 + 3\Delta\xi)$ in which the value $\Delta\xi = 0.01$ is used in this study.

(8) Compute the non-dimensional radius of curvature ζ_j at θ_j using Eq. (43).
(9) After computing all ζ_j at θ_j with $j = 1,2,3,\ldots,n$, compute the $\zeta'_j = (\mathrm{d}\zeta/\mathrm{d}\theta)_j$ using the numerical differentiation method. The result is

$$\zeta'_j = (-25\zeta_j + 48\zeta_{j+1} - 36\zeta_{j+2} + 16\zeta_{j+3} - 3\zeta_{j+4})/(12\Delta\theta). \tag{46}$$

It is noted that in order to obtain the value of $\zeta'_{j=n}$ at the right end ($\theta = \alpha$), the additional number of dividing elements is '4' for applying the forward fourth-order polynomials. See Fig. 3(a).

3.2. Terms of cross-sectional and material properties

Governing equations of Eqs. (23)–(25) are available for the solid- and thin walled-sections, e.g. solid polygon-, wide flanged-, hollowed-sections, etc. The cross-sectional and material properties related to the beam parameters of s, s_p, e, and u are now discussed.

For a given cross-section with the dimensions, cross-sectional properties including k, A, I, I_p, and J can be properly defined and for a given material with the mechanical properties, beam parameters of s, s_p, e, and u in Eqs. (15)–(18) are determined. Although the cross-sections mentioned above can be applied to the parametric studies, the solid rectangular cross-section is selected in the numerical examples of this study. Shown in Fig. 4 is the solid rectangular cross-section with the breadth b and the depth d placed on the horizontal plane (x, y). In this figure, the 1- and 2-axis are the principal ones of the cross-section, which coincide the radial and vertical directions, respectively, of the curved beam.

By the definitions for the cross-sectional properties of a rectangular cross-section, the values of $k = 0.833$, $A = bd$, $I = I_1 = bd^3/12$, $I_p = I_1 + I_2 = (bd^3 + b^3d)/12$, and $J = c_t bd^3$ with $c_t = (1/3)(1-0.63d/b)$ and $d/b \leqslant 1$ [23] are obtained. Substituting all of these values into Eqs. (15)–(18) together with the span length l and the mechanical properties of G and E gives the beam parameters s, s_p, e, and u, or

$$s = 2\sqrt{3}l/d, \quad s_p = s/\sqrt{(b/d)^2 + 1} = s/\sqrt{(1.587 - 0.3968e/g)^{-2} + 1}, \tag{47),(48}$$

$$e = 4(1 - 0.63d/b)g = 4(1 - 0.63/\sqrt{s^2/s_p^2 - 1})g, \quad u = 0.833g, \tag{49),(50}$$

where $g = G/E = 1/[2(1+\nu)]$ and ν is Poisson's ratio. For a computing example, if $l/d = 28.87$, $b/d = 3$ and $\nu = 0.3$, the corresponding values of s, s_p, e, and u are 100, 31.6, 1.22, and 0.32, respectively.

It is now ready to solve the governing equations for calculating the frequency parameter C_i and mode shapes of deformation η_i, ψ_I, and ϕ_i, and those of stress resultants Q_i^*, M_i^*, and T_i^*, respectively.

3.3. Solution method of governing equations

Based on the above analyses, a general FORTRAN program was written for a given set of beam parameters consisting of the beam shape, end constraint, rise ratio f, both slenderness ratios s and s_p, rigidity ratio e,

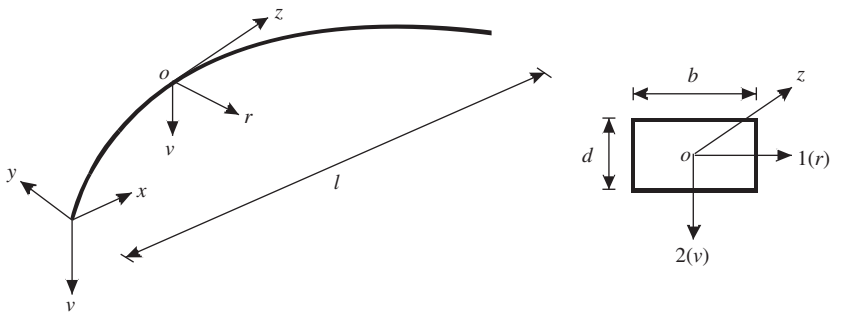

Fig. 4. Coordinates (z, r, v) and solid rectangular cross-section.

shear parameter u and numerical factor c. Recall that the value of c is not available for the parabolic beams (see Fig. 3(a)).

The numerical methods presented by Lee and Wilson [21] were used to solve the differential equations. First, the Runge–Kutta method [22] was used to integrate the differential equations of Eqs. (23)–(25) from $\theta = 0$ to α subject to the boundary conditions from either Eqs. (26)–(28) or Eqs. (29)–(31) according to the given end constraint. From the results of the Runge–Kutta solutions, the deformations of η, ψ, and ϕ accompanied with their corresponding derivatives η', ψ', and ϕ' are obtained. Second, the determinant search method [21] combined with the Regula–Falsi method [22] was used to determine the eigenvalues C_i of the governing equations, which satisfy the boundary conditions of either Eqs. (26)–(28) or Eqs. (29)–(31) at the right end ($\theta = \alpha$). Finally, mode shapes of the stress resultants Q_i^*, M_i^*, and T_i^* are calculated by Eqs. (32)–(34).

4. Numerical examples and discussion

In numerical examples of this study, three kinds of beam shapes of the parabolic, sinusoidal and elliptic beams and three kinds of end constraints of the hinged–hinged, hinged–clamped, and clamped–clamped ends are considered. The beam parameters of f, s, s_p, e, u, and c are examined in the parametric studies concerning calculations of the frequency parameters and mode shapes. In parametric studies of this study, the cross-section of the beam is only limited in the solid rectangular cross-section (see Section 3.2).

Prior to showing the numerical examples, the convergence analysis for the parabolic beam with hinged–clamped ends, $f = 0.2$, $s = 100$, $s_p = 31.6$, $e = 1.22$, and $u = 0.32$ was carried out for determining the suitable step size $\Delta\theta$ to be used in the Runge–Kutta scheme. As indicated by results in Table 1, the values of C_i with $\alpha/\Delta\theta = 50$ are sufficiently close to those with $\alpha/\Delta\theta = 200$. To ensure accuracy of solutions, the value of $\alpha/\Delta\theta = 100$ is used throughout the parametric studies.

The numerical results, given in Tables 2–4 and Figs. 5–8, are now discussed. Shown in Table 2 is the effect of beam shapes on frequency parameters C_i. The discrepancies of C_i between three beam shapes with $c = 0.1$ and 0.5 (except parabolic beams) are relatively little from each other since the deviations of $\delta(\xi)$ between three beam shapes are relatively little. However, it is expected that the discrepancies of C_i become to be large as each value of c becomes to be largely deviated.

Table 3 shows effects of the rotatory and torsional inertias on C_i, in which E_R and E_T are the rotatory and torsional inertia indices, respectively. If the rotatory inertia is excluded, the index E_R is 0, and if included, E_R is 1. Also, if the torsional inertia is excluded, $E_T = 0$, and if included, $E_T = 1$. When the rotatory and torsional inertias are excluded, the coefficients of $s^{-2}C_i^2\zeta^2$ in Eq. (24) and $s_p^{-2}C_i^2\zeta^2$ in Eq. (25), which are related to the rotatory and torsional inertias, respectively, are merely deleted. In Table 3, the beam shape is sinusoidal; the end constraints are hinged–hinged, hinged–clamped, and clamped–clamped; and the beam parameters are $f = 0.2$, $s = 100$, $s_p = 31.6$, $e = 1.22$, $u = 0.32$, and $c = 0.5$. The inclusions of both rotatory and torsional inertias always result in reduction of the C_i values. It is apparent that if the torsional inertia is excluded

Table 1
Convergence study for parabolic beam with hinged–clamped ends[a]

$\frac{\alpha}{\Delta\theta}$	Frequency parameter, C_i						
	$i = 1$	$i = 2$	$i = 3$	$i = 4$	$i = 5$	$i = 6$	$i = 7$
10	10.43	43.07	92.30	109.7	161.1	203.8	252.0
20	11.06	38.87	83.46	109.7	141.4	203.9	215.0
50	11.15	39.08	82.59	109.8	141.4	204.0	213.8
100	11.15	39.10	82.61	109.8	141.4	204.0	213.8
200	11.15	39.10	82.61	109.8	141.4	204.0	213.8

[a] $f = 0.2$, $s = 100$, $s_p = 31.6$, $e = 1.22$, and $u = 0.32$.

Table 2
Effect of beam shape on frequency parameter, C_i[a]

End constraint	Beam shape	Parameter, c	Frequency parameter, C_i						
			$i=1$	$i=2$	$i=3$	$i=4$	$i=5$	$i=6$	$i=7$
Hinged–hinged	Parabolic[b]	–	6.090	30.40	70.03	109.8	125.0	194.0	203.8
	Sinusoidal	0.1	6.443	31.11	70.12	111.5	125.8	195.3	204.8
		0.5	6.215	30.65	70.15	110.3	125.4	194.5	203.8
	Elliptic	0.1	5.340	28.83	67.74	107.9	121.7	189.3	203.6
		0.5	5.905	30.03	69.72	109.1	124.4	193.1	203.7
Hinged–clamped	Parabolic	–	11.15	39.10	82.61	109.8	141.4	203.8	213.8
	Sinusoidal	0.1	11.38	39.61	82.64	111.6	142.2	204.1	215.3
		0.5	11.24	39.29	82.71	110.3	141.8	203.8	214.4
	Elliptic	0.1	10.69	37.87	80.51	107.9	138.1	203.5	209.1
		0.5	11.04	38.82	82.33	109.1	140.7	203.7	212.9
Clamped–clamped	Parabolic	–	17.12	48.77	96.06	109.9	158.7	203.8	234.7
	Sinusoidal	0.1	17.17	49.24	95.70	112.1	159.5	204.1	236.2
		0.5	17.14	48.95	96.05	110.6	159.0	203.9	235.3
	Elliptic	0.1	17.02	47.83	94.07	108.0	158.0	203.6	229.8
		0.5	17.10	48.53	95.87	109.2	158.0	203.7	233.7

[a]$f=0.2$, $s=100$, $s_p=31.6$, $e=1.22$, and $u=0.32$.
[b]In parabolic beams, the parameter c is not available.

Table 3
Effects of rotatory (E_R) and torsional (E_T) inertias on frequency parameter, C_i[a]

End constraint	E_R[b]	E_T[c]	Frequency parameter, C_i						
			$i=1$	$i=2$	$i=3$	$i=4$	$i=5$	$i=6$	$i=7$
Hinged–hinged	0	0	6.227	30.77	70.77	126.6	196.9	280.8	377.2
	1	0	6.224	30.72	70.52	125.8	195.1	277.3	371.3
	0	1	6.217	30.70	70.39	**110.3**	126.1	196.3	**203.8**
	1	1	6.215	30.65	70.15	**110.3**	125.4	194.5	**203.8**
Hinged–clamped	0	0	11.26	39.46	83.49	143.1	217.1	304.5	403.5
	1	0	11.26	39.39	83.19	142.2	215.1	300.7	397.9
	0	1	11.24	39.35	83.01	**110.3**	142.6	**203.8**	216.4
	1	1	11.24	39.29	82.71	**110.3**	141.8	**203.8**	214.4
Clamped–clamped	0	0	17.19	49.18	97.18	160.6	238.2	329.1	431.6
	1	0	17.18	49.09	96.81	159.6	236.0	325.0	425.2
	0	1	17.15	49.04	96.40	**110.6**	160.1	**203.8**	237.5
	1	1	17.14	48.95	96.05	**110.6**	159.0	**203.8**	235.3

[a]Sinusoidal beam, $f=0.2$, $s=100$, $s_p=31.6$, $e=1.22$, $u=0.32$, and $c=0.5$.
[b]If $E_R=0$, all vibration modes are flexible.
[c]Bold lettered figures: torsional modes; not bold lettered figures: flexural modes.

($E_T=0$), the C_i values for the torsional modes cannot be obtained explicitly. Therefore, it is true that if $E_T=0$, the Eqs. (23)–(25) are reduced to differential equations governing only the free flexural vibrations of beam with variable curvature. In Table 3, the torsional frequencies are written as bold lettered figures while the flexural ones as not bold lettered. As can be seen, if $E_T=1$, torsional frequencies $C_4=110.3$ of hinged–hinged and hinged–clamped ends, and $C_4=110.6$ of clamped–clamped ends are nearly the same but not identical.

Table 4
Effect of elasticity ratio $g(=G/E)$ on frequency parameter, C_i[a]

End constraint	Elasticity ratio, g	Frequency parameter, C_i						
		$i=1$	$i=2$	$i=3$	$i=4$	$i=5$	$i=6$	$i=7$
Hinged–hinged	0.30	5.769	29.80	69.28	**98.68**	123.5	**181.0**	191.2
	0.35	5.856	29.95	69.57	**105.0**	124.1	192.4	**194.7**
	0.40	5.920	30.06	69.79	**111.0**	124.6	193.3	**207.5**
	0.45	5.980	30.15	69.96	**116.6**	124.9	194.0	**219.6**
	0.50[b]	6.025	30.22	70.09	**122.0**	125.2	194.6	**231.0**
Hinged–clamped	0.30	10.93	38.58	81.82	**98.69**	139.7	**181.0**	210.8
	0.35	11.00	38.73	82.15	**105.0**	140.4	**194.7**	212.2
	0.40	11.05	38.85	82.40	**111.0**	140.9	**207.5**	213.2
	0.45	11.10	38.94	82.59	**116.6**	141.3	214.0	**219.6**
	0.50	11.13	39.01	82.74	**122.0**	141.6	214.6	**231.0**
Clamped–clamped	0.30	17.01	48.29	95.19	**98.82**	156.8	**181.0**	231.3
	0.35	17.06	48.45	95.66	**105.0**	157.6	**194.7**	232.8
	0.40	17.11	48.57	95.95	**111.0**	158.2	**207.5**	234.0
	0.45	17.14	48.66	96.17	**116.6**	158.6	**219.6**	234.9
	0.50	17.17	48.74	96.34	**122.0**	159.0	**231.0**	235.6

Bold lettered figures are torsional frequencies.
[a]Elliptic beam, $f=0.2$, $s=100$, $s_p=31.6$, $e=3.16g$, $u=0.833g$, and $c=0.5$.
[b]Practically not possible but theoretically largest value.

Also, if $E_T=1$, $C_7=203.8$ of hinged–hinged ends and $C_6=203.8$ of hinged–clamped and clamped–clamped ends are the same. This means that the hinged and clamped ends should play a role similarly in determining the torsional frequencies. Hereafter, both the rotatory and torsional inertias are included in the parametric studies to be discussed.

Table 4 shows effects of the elasticity ratio g or shear parameter $u(=kg)$ on the C_i. Here, the beam parameters are elliptic beam, $f=0.2$, $s=100$, $s_p=31.6$, and $c=0.5$. Recall that the rigidity ratio $e=4(1-0.63/\sqrt{s^2/s_p^2-1})g$ in Eq. (49) depends on the value of s, s_p and g. Therefore, according to the values of $s=100$ and $s_p=31.6$, the value e becomes to be $e=3.16g$. For the rectangular cross-section, the shape factor k is 0.833 so that $u=0.833g$. Meanwhile, value of g for the structural materials approximately ranges from 0.3 to less than 0.5. It is observed that the C_i value increases as the g (or u) value increases. For fictitiously very large value of g, the effect of shear deformation should be neglected because the shear distortion β in Eq. (4) approaches zero and consequently, the total rotation of the cross-section $v'/\rho=\psi+\beta$ consists of only the rotation ψ due to pure bending. Therefore, the C_i value is clearly overestimated unless the shear deformation is included. In Table 4, the torsional frequencies are presented as the bold lettered figures for reader's convenience. It is true that the effect of g is more pronounced for the torsional frequencies than the flexural ones. For an example, the ratios of C_i with $g=0.5$ to C_i with $g=0.30$ are 1.236 ($=122.0/98.68$) of the torsional mode ($i=4$ and bold lettered figure) and 1.014 ($=125.2/123.5$) of the flexural one ($i=5$), respectively, for the hinged–hinged ends.

Shown in Fig. 5 is C_i versus f curves for parabolic beam with (a) hinged–hinged, (b) hinged–clamped, and (c) clamped–clamped ends. The beam parameters are: $s=100$, $s_p=31.6$, $e=1.22$ and $u=0.32$. The C_i value decreases as the value of f increases. In cases of the hinged–hinged and clamped–clamped ends, the mode shapes are either symmetric or anti-symmetric since geometry of the beam including the end constraint is symmetric. However, the same is not true for the beam with hinged–clamped ends, because the end constraint is not symmetric, although the geometry is symmetric. For the hinged–hinged and clamped–clamped ends in Fig. 5(a) and (c), respectively, the symmetric modes are depicted as 'S' and anti-symmetric ones as 'A,' As discussed in Table 3, the vibration modes are either flexural or torsional. Also, in Fig. 5(a), (b) and (c), the

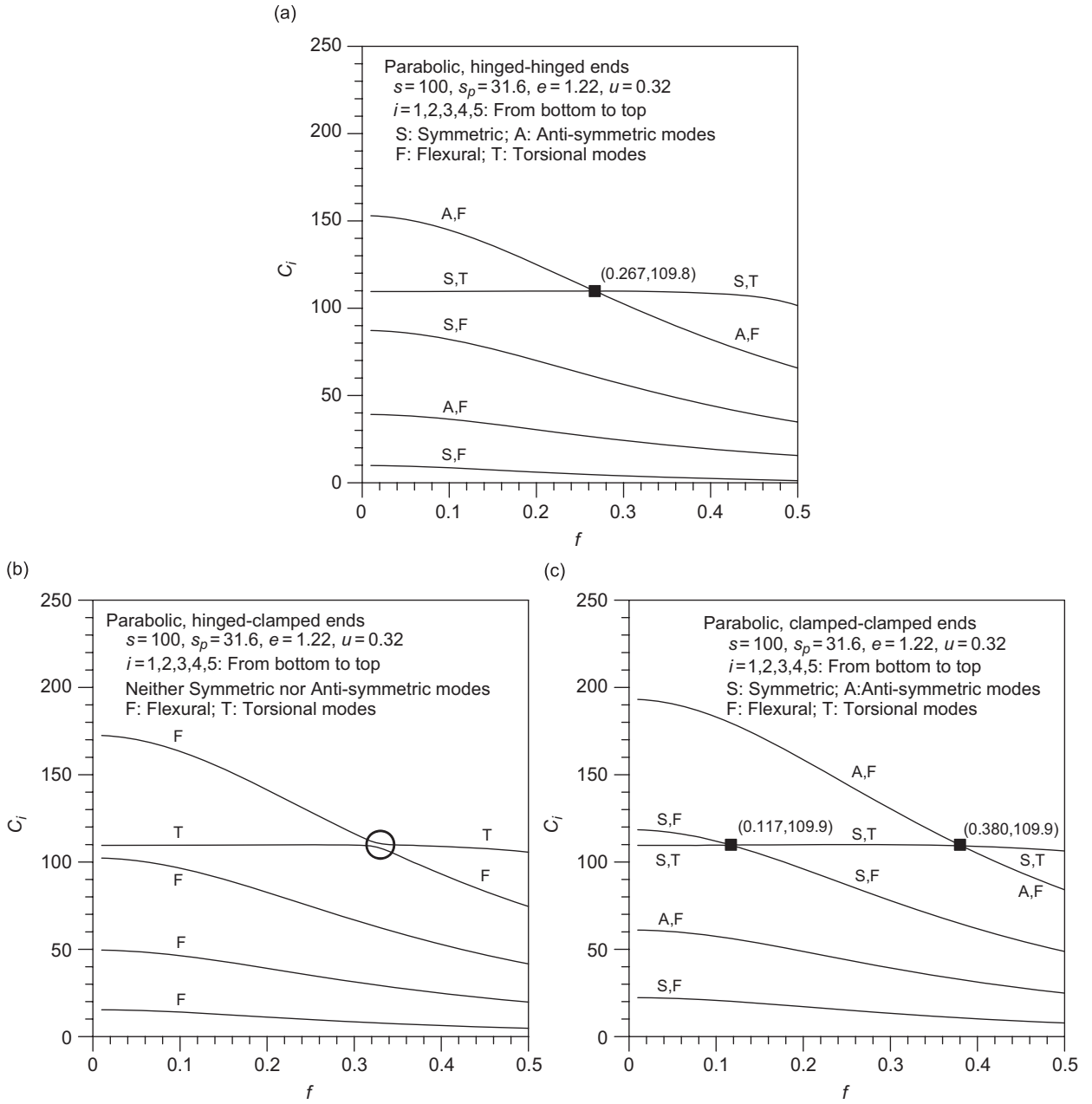

Fig. 5. The C_i versus f curves for parabolic beam with (a) hinged–hinged, (b) hinged–clamped, and (c) clamped–clamped ends.

flexural and torsional modes are depicted as 'F' and 'T,' respectively. In Fig. 5(a) and (c), two vibration modes exist at a single frequency parameter where two frequency curves meet at the coordinates (f, C_i) marked by ■. For an example, the fourth and fifth modes of the hinged–hinged ends in Fig. 5(a) have the same frequencies $C_4 = C_5 = 109.8$ at $f = 0.267$. As can be seen, for $f < 0.267$, the fourth mode is symmetric and torsional, and the fifth mode is anti-symmetric and flexural. The two pairs of mode shapes switch at the coordinates of (0.267, 109.8) marked by ■ so that for $f > 0.267$, the fourth mode becomes to be anti-symmetric and flexural, and the fifth mode becomes to be symmetric and torsional. For the hinged–clamped ends in Fig. 5(b), the fourth and fifth frequency curves only approach each other but not cross in the range of f sectioned by the figure of ○. Although two curves do not meet, the vibration modes clearly shift before and after this range,

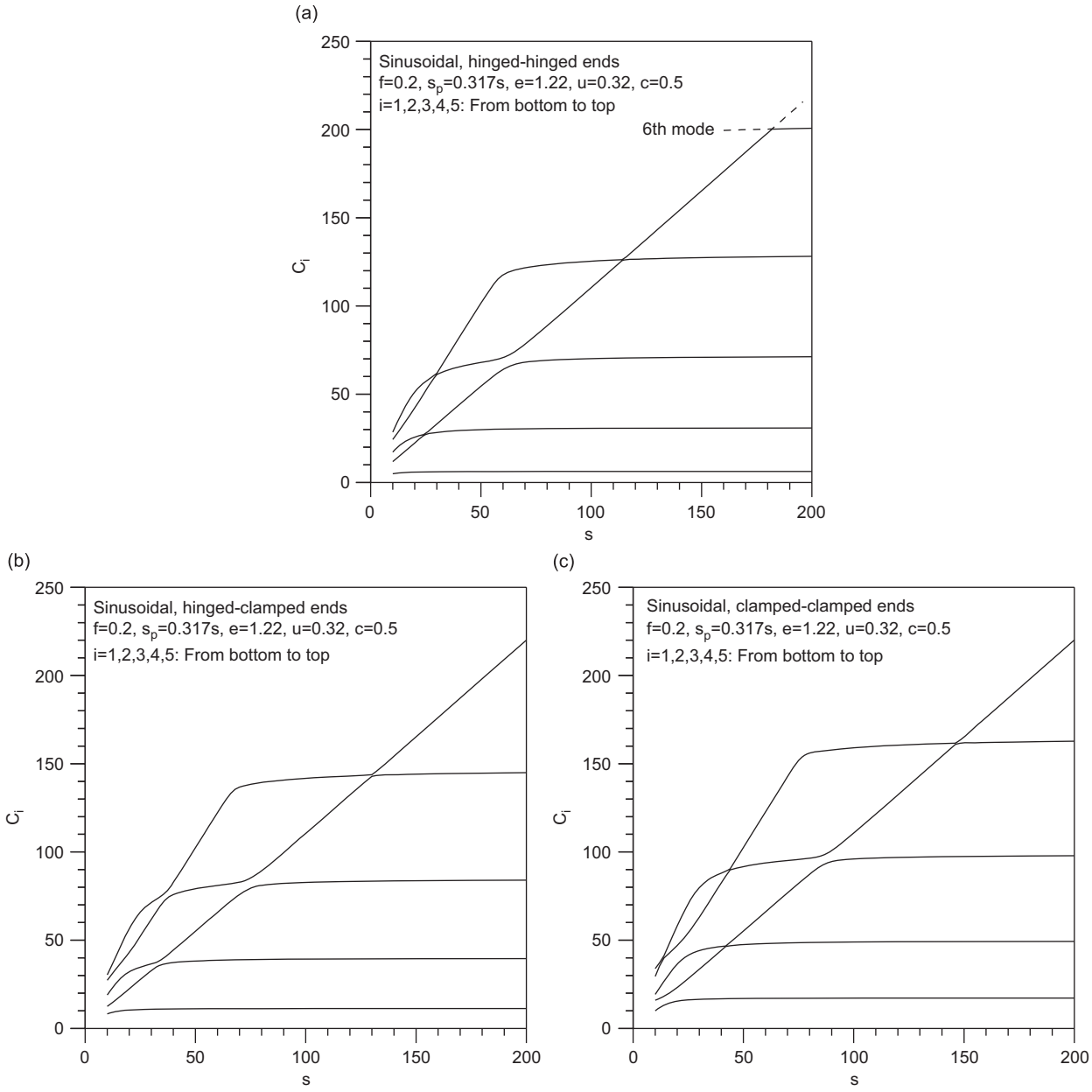

Fig. 6. The C_i versus s curves for sinusoidal beam with (a) hinged–hinged, (b) hinged–clamped, and (c) clamped–clamped ends.

which is the transition range of the vibration modes. For the clamped–clamped ends in Fig. 5(c), there are two shifting points marked by ■. It is clear that in these three figures, the diagonal frequency curves are flexural while the horizontal ones are torsional, and the effect of f on the C_i of torsional vibration is very lesser.

Fig. 6 shows the effect of s on C_i for sinusoidal beam with (a) hinged–hinged, (b) hinged–clamped and (c) clamped–clamped ends. The beam parameters are: $f = 0.2$, $s_p = 0.317s$, $e = 1.22$, $u = 0.32$, and $c = 0.5$, in which the relationship between s_p and s with $e = 1.22$ becomes to be $s_p = 0.317s$. See Eq. (49). It is apparent that the C_i value increases and approaches an asymptote as the value of s increases. Both terms of $u^{-1}s^{-2}C_i^2\zeta^2\eta$ in Eq. (23) and $s^{-2}C_i^2\zeta^2\psi$ in Eq. (24) are originated from the transverse inertia force F_v and rotatory inertia couple C_ψ related to the flexural mode so that the diagonal frequency curves which vary deeply with s are the flexural modes clearly and meanwhile, the horizontal curves which vary very gently with s are the torsional

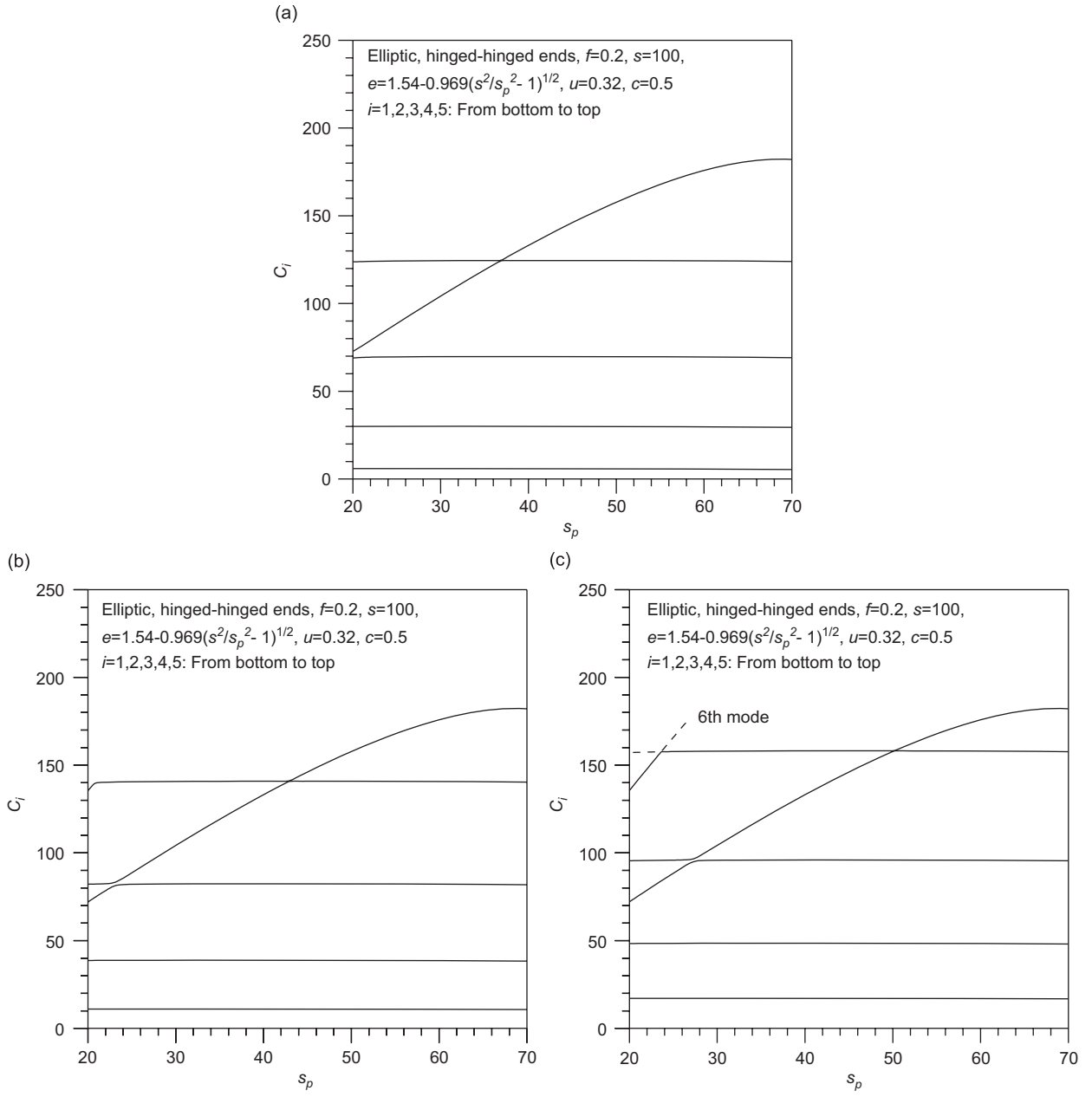

Fig. 7. The C_i versus s_p curves for elliptic beam with (a) hinged–hinged, (b) hinged–clamped, and (c) clamped–clamped ends.

ones. It is true that the effect of slenderness s on C_i of the torsional modes is negligible. In addition, the transition ranges also exist in these frequency curves as already shown in Fig. 5(c). The sixth frequency curve in Fig. 6(a) is presented in part as the dashed line to show being the coordinates (s, C_i) where the mode shift is occurred.

Shown in Fig. 7 is the relationship between C_i and s_p for the elliptic beam with (a) hinged–hinged, (b) hinged–clamped, and (c) clamped–clamped ends. The beam parameters are $f = 0.2$, $s = 100$, $e = 1.54-0.969/(s^2/s_p{}^2-1)^{1/2}$, $u = 0.32$, and $c = 0.5$. The frequency curves in the Fig. 7 are presented in the range of $s_p \geqslant 20$ because the minimal value of s_p is approximately '20' in order to meet the condition of $d/b \leqslant 1$. See Eq. (49). The C_i value increases and converges to some asymptote as the value of s_p increases. The term of $s_p{}^{-2}C_i{}^2\zeta^2\phi$ in

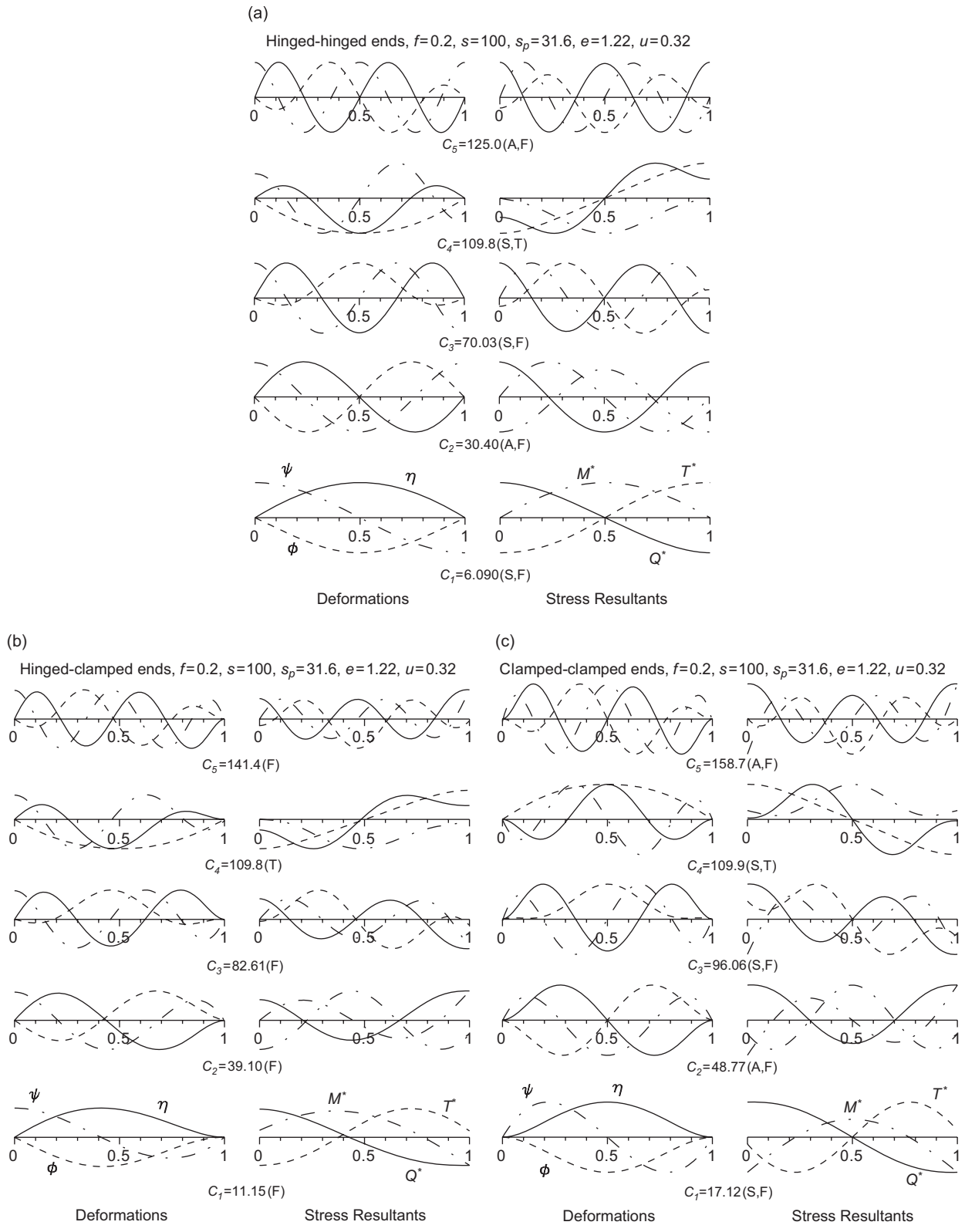

Fig. 8. Mode shapes for parabolic beam with (a) hinged–hinged, (b) hinged–clamped, and (c) clamped–clamped ends.

Eq. (25) is originated from the torsional inertia moment C_ϕ in Eq. (25) related to the torsional vibration so that the diagonal frequency curves are the torsional modes and the horizontal curves are the flexural ones. It is natural that the effect of slenderness s_p on C_i of the flexural vibrations is negligible. Also, the transition ranges exist in these frequency curves as already shown in Figs. 5(c) and 6. The sixth frequency curve in Fig. 7(c) is presented in part as the dashed line to show being the coordinates (s_p, C_i) where the mode shift is occurred.

Fig. 8 shows the typical examples of mode shapes of deformations of η_i, ψ_i, and ϕ_i, and stress resultants of, Q_i^*, M_i^* and T_i^* for the parabolic beams with (a) hinged–hinged, (b) hinged–clamped and (c) clamped–clamped ends. The beam parameters are $f = 0.2$, $s = 100$, $s_p = 31.6$, $e = 1.22$, and $u = 0.32$. The mode shapes with their corresponding frequencies in these figures can be classified as follows:

(a) Parabolic beam with hinged–hinged ends:
- First mode: symmetric and flexural ($C_1 = 6.090$).
- Second mode: anti-symmetric and flexural ($C_2 = 30.40$).
- Third mode: symmetric and flexural ($C_3 = 70.03$).
- Fourth mode: symmetric and torsional ($C_4 = \mathbf{109.8}$).
- Fifth mode: anti-symmetric and flexural ($C_5 = 125.0$).

(b) Parabolic beam with hinged–clamped ends (neither symmetric nor anti-symmetric):
- First mode: flexural ($C_1 = 11.15$).
- Second mode: flexural ($C_2 = 39.10$).
- Third mode: flexural ($C_3 = 82.61$).
- Fourth mode: torsional ($C_4 = \mathbf{109.8}$).
- Fifth mode: flexural ($C_5 = 141.4$).

(c) Parabolic beam with clamped–clamped ends:
- First mode: symmetric and flexural ($C_1 = 17.12$).
- Second mode: anti-symmetric and flexural ($C_2 = 48.77$).
- Third mode: symmetric and flexural ($C_3 = 96.06$).
- Fourth mode: symmetric and torsional ($C_4 = \mathbf{109.9}$).
- Fifth mode: anti-symmetric and flexural ($C_5 = 158.7$).

It is seen that the fourth torsional mode shapes of hinged–hinged ends in Fig. 8(a), hinged–clamped ends in Fig. 8(b) and clamped–clamped ends in Fig. 8(c) quite differ with each other, especially those of rotation ψ, even though the three torsional frequencies are nearly identical, namely $C_4 = 109.8$, 109.8, and 109.9. From the mode shapes depicted in Fig. 8, the positions of maximum amplitudes and interior nodal points for both deformations and stress resultants can be observed, which can serve as useful reference for the design of curved beams especially when the dynamic loads are subjected.

Since the mode shapes of deformations v,ψ, and ϕ are either symmetric or anti-symmetric for cases of the hinged–hinged and clamped–clamped ends, the boundary conditions at the mid-arc ($\theta = \alpha/2$) are obtained from results of the mode shapes shown in Fig. 8(a) and (c), or

- Symmetric mode:

$$\eta' = 0, \quad \psi = 0, \quad \phi' = 0. \tag{51)–(53}$$

- Anti-symmetric mode:

$$\eta = 0, \quad \psi' = 0, \quad \phi = 0. \tag{54)–(56}$$

The frequency parameters C_i can be obtained by using the boundary conditions at the mid-arc ($\theta = \alpha/2$) of Eqs. (51)–(53) and Eqs. (54)–(56) rather than the boundary conditions of Eqs. (26)–(31) at the right end ($\theta = \alpha$) already discussed in Chapter 2. It is fact that both results of the values of C_i are the same each other (not shown herein).

5. Experimental methods and measured results

Laboratory-scale aluminum, parabolic curved beams were designed and tested for a hinged–hinged, a hinged–clamped, and a clamped–clamped end constraint. These curved beams all had the same geometry: $l = 0.346\,\text{m}$, $h = 0.104\,\text{m}$ and solid rectangular cross-section with $b = 0.03\,\text{m}$ and $d = 0.006\,\text{m}$. And the material properties of aluminum are mass density $\gamma = 2680\,\text{kg/m}^3$, shear modulus of elasticity $G = 2.60 \times 10^{10}\,\text{N/m}^2$ and Young's modulus $E = 6.89 \times 10^{10}\,\text{N/m}^2$. The cross-sectional properties of the specimen beams are now calculated: $A = 1.8 \times 10^{-4}\,\text{m}^2$, $I = 5.4 \times 10^{-10}\,\text{m}^4$, $I_p = 1.404 \times 10^{-8}\,\text{m}^4$, and $J = 1.888 \times 10^{-9}\,\text{m}^4$. Recall that $k = 0.833$ for the solid rectangular cross-section. Therefore, the corresponding non-dimensional beam parameters are: $f = 0.3$ ($\alpha = 1.752\,\text{rad.}$), $s = 200$, $s_p = 39.2$, $e = 1.319$, $u = 0.314$ with which the frequency parameters C_i for each of the three end constraints were calculated by the theory developed herein. With these values of C_i, the corresponding frequencies ω_i were calculated from Eq. (13). The predicted natural frequencies for experimental beams are thus $F_i = \omega_i/(2\pi) = 73.36C_i/(2\pi) = 11.68C_i\,\text{Hz}$.

Fig. 9 shows (a) a side view of the experimental setup, and (b) the modal analysis system used to measure C_i for the curved beams in out-of-plane free vibration. The end of a model beam was either fastened to a steel hinge or clamped between the steel blocks, both of which were anchored with bolts to a 5 cm thick acryl slab glued rubber pad of medium stiffness. This experimental design provided low heave and rotational frequencies

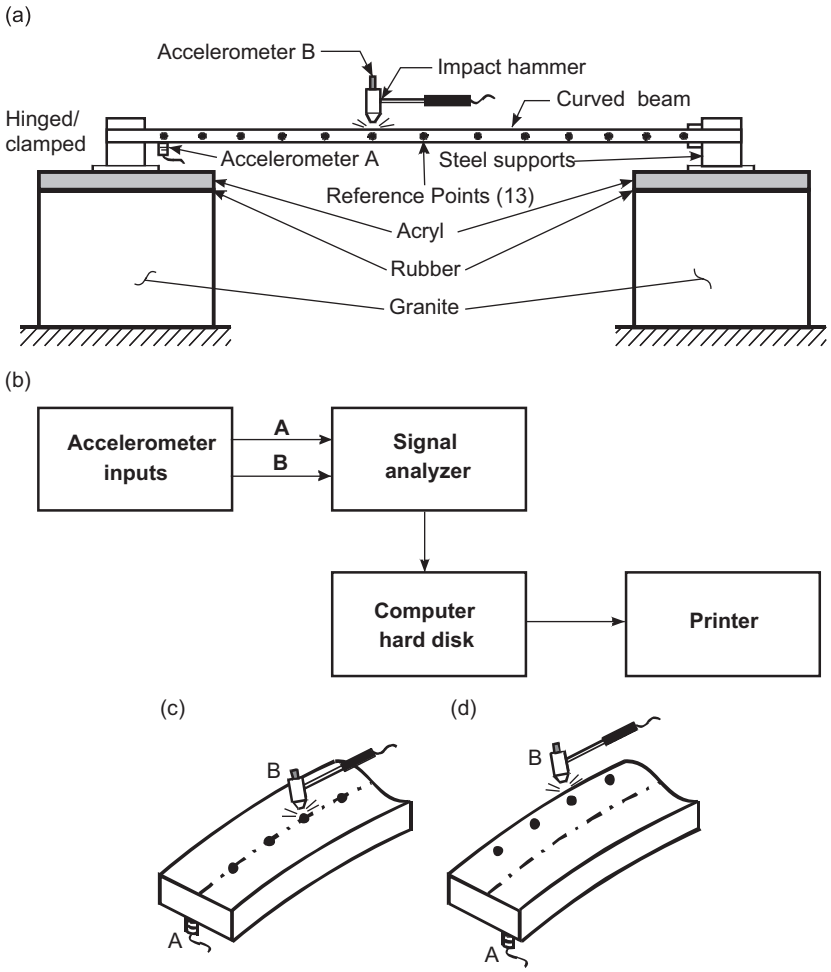

Fig. 9. Schematic drawings: (a) experimental setup; (b) modal analysis system, (c) exciting only flexural modes, and (d) exciting both flexural and torsional modes.

for each granite block, and offered vibration isolation at the ends. This design minimized the effect of vibration on the end supports so that the experimental frequencies of the beam itself could be identified easily [12,21].

In the experiments, 13 reference points were evenly spaced along the top of each beam. As shown in Fig. 9(a), a miniature piezoelectric accelerometer, A, was affixed to the underside of the beam at the reference point nearest to one end. In a typical experiment, each reference point was struck vertically at the top of the beam with an impact hammer, which was fitted with a miniature accelerometer, B. For each test, a record of the time history of the out-of-plane response for both accelerometers A and B was obtained. All data were received by a Signal Analyzer (Model SD390, Scientific-Atlanta Corporation) and processed through a minicomputer using a fast Fourier transform analyzer as shown in Fig. 9(b). For data collected for a hammer blow at the location of accelerometer A, the software was used to calculate the frequency spectrum. The peaks of this spectrum occur at the free vibration frequencies of the beam. The reader should be referred to the work of Ewins [24] for more details on the methods of data processing.

Note that for measuring only the flexural vibration, the accelerometer A was affixed to the breadth's mid-point of the bottom surface of the beam and the reference points which were marked along the center line at the top surface of the beam were struck by the hammer with an accelerometer B, while for measuring both the flexural and torsional vibrations simultaneously, the accelerometer A was affixed to an inner point from the breadth's mid-point and the hammer strikes were done along the reference points marked along the outer side from the center line of the beam. See Fig. 9(c) and (d). From two separate experiments, the measured frequencies can easily be classified into the flexural or torsional modes [12].

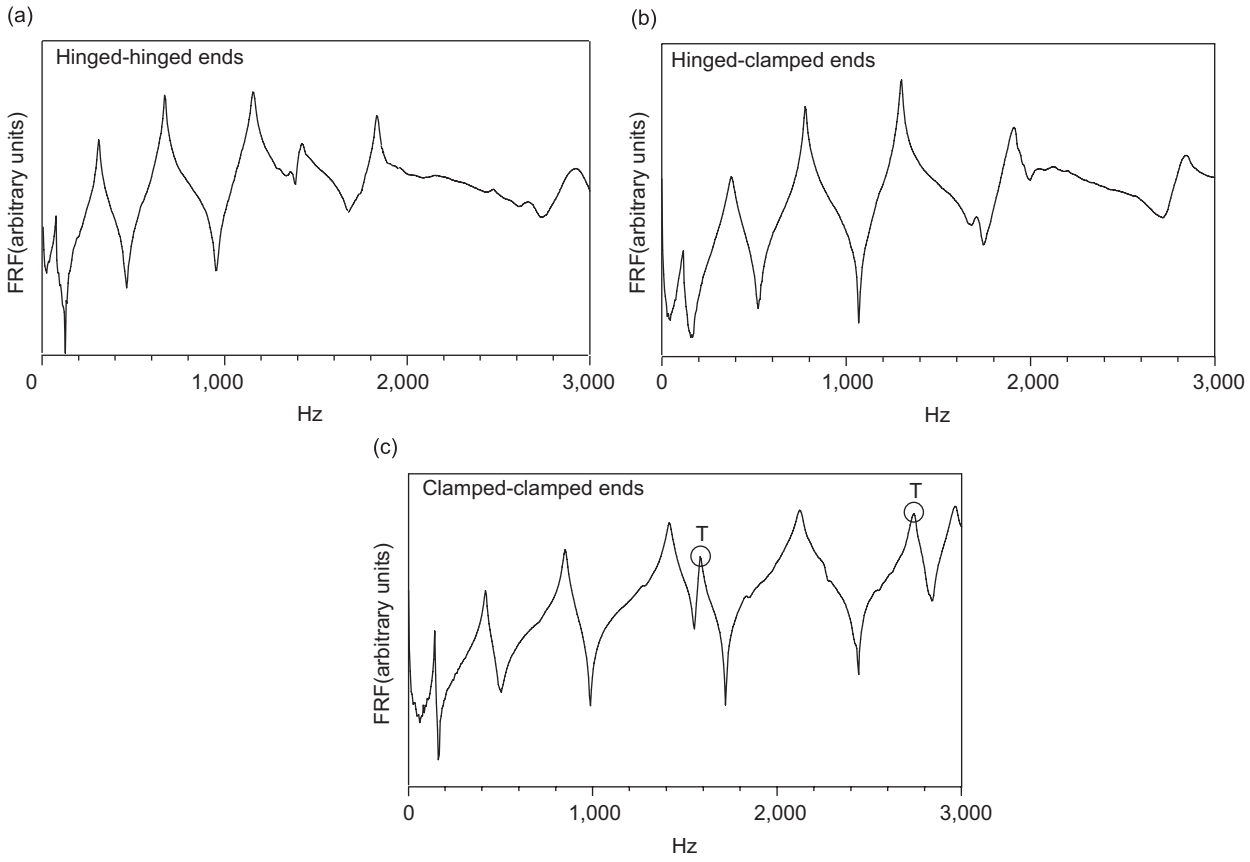

Fig. 10. Free vibration acceleration spectra for the three experimental parabolic beams: (a) hinged–hinged, (b) hinged–clamped, and (c) clamped–clamped ends.

The frequency spectrums for each of the three beams that were tested are presented in Fig. 10(a)–(c) for the case where both the flexural and torsional modes were simultaneously measured. The software gave a listing of the seven lowest frequencies corresponding to the seven first peaks of each spectrum. These results, which were reproduced to within about 2% in repeated tests, are the experimental frequencies listed in Table 5 where the predicted frequencies calculated in this study are also presented. In addition, natural frequencies obtained by the finite element program ADINA for the three experimental beams are listed in Table 5 for the comparison purpose.

Table 5
Comparison of natural frequencies, F_i (Hz) between this study, ADINA and experiment for parabolic beams

End constraint	i	This study		ADINA	Experiment	Deviation (%)[a]
		C_i	F_i (Hz)	F_i (Hz)	F_i (Hz)	
Hinged–hinged	1	3.971	46.38	46.23	55.95	17.1
	2	24.40	284.9	284.1	269.6	5.7
	3	57.09	666.8	664.9	589.3	13.2
	4	104.4	1219.	1216.	1099.	10.9
	5	**139.8**[b]	**1633.**	**1626.**	**1597.**	2.3
	6	164.7	1923.	1917.	1943.	1.0
	7	**236.7**	**2764.**	**2748.**	**2953.**	6.4
Hinged–clamped	1	8.444	98.63	98.33	119.2	17.3
	2	31.51	368.1	367.0	376.4	2.2
	3	67.72	790.9	788.7	778.2	1.6
	4	118.3	1381.	1378.	1312.	5.3
	5	**139.8**[b]	**1633.**	**1626.**	**1695.**	3.7
	6	181.9	2124.	2122.	1907.	11.5
	7	**241.9**	**2825.**	**2814.**	**2792.**	1.2
Clamped–clamped	1	13.37	156.1	155.7	142.4	9.6
	2	39.55	461.9	460.6	417.1	10.7
	3	79.09	923.8	921.1	849.4	8.8
	4	133.1	1554.	1550.	1409.	10.3
	5	**139.8**	**1633**	**1626.**	**1582.**	3.2
	6	200.0	2335.	2327.	2121.	10.1
	7	**242.4**	**2831.**	**2816.**	**2741.**	3.3

[a]Deviation (%) = |1–this study/experiment| × 100.
[b]Bold lettered figures are torsional frequencies.

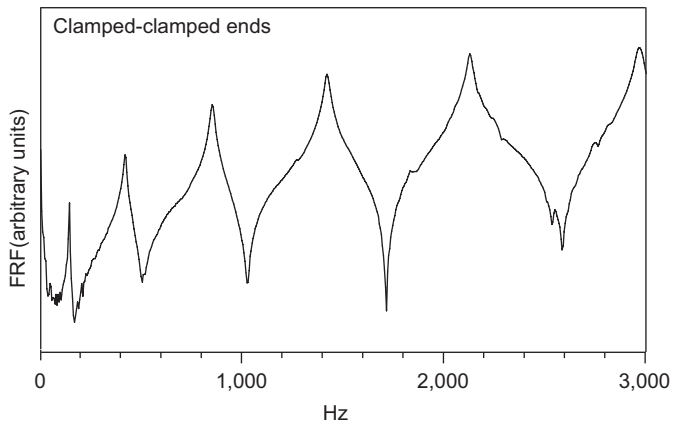

Fig. 11. Free vibration acceleration spectra for the clamped–clamped parabolic beam exciting only flexural vibration.

This table shows two results of this study and ADINA are nearly identical. This validates the mathematical model and numerical method developed herein. Also, this table shows excellent agreements between the two results obtained from this study and experiment. For the three beams, the percentage deviations between this study and experiment in the results average about 7.4%. It is noted that high peaks in Fig. 10(a)–(c) exist for all three transfer functions near the zero frequency. It is undoubtedly due to the rocking responses of the 30 kg granite blocks, which rested on the rubber pads at the ends of the beam. This assemble has relatively low natural frequencies of about 2 Hz.

For reader's convenience, the frequency spectrum for the clamped–clamped beam that was tested is presented in Fig. 11 for the case where the flexural vibration was only measured. Comparing two figures (Figs. 10(c) and 11), it is clear that two natural frequencies of $F_5 = 1582$ and $F_7 = 2741$, marked by 'T,' in Fig. 10(c) are the torsional frequencies, whose peaks are not appeared in Fig. 11.

6. Concluding remarks

The differential equations governing the free, out-of-plane vibrations of horizontally curved beams with variable curvature are derived in which the effects of rotatory and torsional inertias and shear deformation are included. The differential equations are solved numerically to calculate the frequency parameters accompanied with the mode shapes. In the numerical examples, the parabolic, sinusoidal and elliptic beams with hinged–hinged, hinged–clamped, and clamped–clamped end constraints are considered. The inclusions of rotatory and torsional inertias always result in reduction of the frequency parameters. If the torsional inertia is excluded, the frequency parameters of torsional modes cannot be obtained. The frequency parameter C_i increases as the value of the shear parameter u (or elasticity ratio g) increases. The C_i values are overestimated if the shear deformation is excluded. The effects of beam parameters on the frequency parameters are intensively investigated: the C_i value decreases as the rise ratio f increases, and it increases as the slenderness ratios s and s_p increase. Typical mode shapes of the stress resultants as well as deformations are presented. The natural frequencies obtained by experiments agree closely with those obtained by theories developed herein.

Both mathematical and numerical methods presented herein are robust and reliable in calculating the natural frequencies accompanying with the mode shapes for curved beams with variable curvature, which can be extensively utilized in designing the curved beams.

Acknowledgment

The first author thanks for the financial support provided by the Wonkwang University, Korea in 2007.

References

[1] A.K. Gupter, W.P. Howson, Exact natural frequencies of plane structures composed of slender elastic curved member, *Journal of Sound and Vibration* 175 (1994) 145–157.

[2] W.P. Howson, A.K. Jemah, J.Q. Zhou, Exact natural frequencies for out-of-plane motion of plane structure composed of curved beam member, *Computers and Structures* 55 (1995) 989–995.

[3] W.P. Howson, A.K. Jemah, Exact out-of-plane natural frequencies of curved Timoshenko beams, *Journal of Engineering Mechanics—ASCE* 125 (1999) 19–25.

[4] T.M. Wang, M.P. Guilbert, Effects of rotatory inertia and shear on natural frequencies of continuous circular curved beams, *International Journal of Solids and Structures* 17 (1981) 281–289.

[5] M.S. Issa, T.M. Wang, B.T. Hsiao, Extensional vibrations of continuous circular curved beams with rotatory inertia and shear deformation I: free vibration, *Journal of Sound and Vibration* 114 (1987) 297–308.

[6] K.J. Kang, C.W. Bert, A.G. Striz, Vibration analysis of horizontally curved beams with warping using DQM, *Journal of Structural Engineering—ASCE* 122 (1996) 657–662.

[7] T.M. Wang, Fundamental frequency of clamped elliptic arcs for vibration outside the plane of initial curvature, *Journal of Sound and Vibration* 42 (1975) 515–519.

[8] S. Takahashi, K. Suzuki, Vibrations of elliptic arc bar perpendicular to their plane, *Bulletin of the Japan Society of Mechanical Engineers* 20 (1977) 1409–1416.

[9] J.F.M. Scott, J. Woodhouse, Vibration of an elastic strip with varying curvature, *Philosophical Transactions of the Royal Society of London Physical Science and Engineering* 339 (1992) 587–625.

[10] A.S. Gendy, A.F. Saleeb, Vibration analysis of coupled extensional/flexural/torsional modes or curved beams with arbitrary thin-walled sections, *Journal of Sound and Vibration* 174 (1994) 261–274.
[11] M. Kawakami, T. Sakiyama, H. Matsuda, C. Morita, In plane and out-of-plane free vibrations of curved beams with variable sections, *Journal of Sound and Vibration* 187 (1995) 381–401.
[12] B.K. Lee, T.E. Lee, A.J. Carr, S.J. Oh, Out-of-plane free vibrations of circular strips with variable breadth, *International Journal of Structural Stability and Dynamics* 7 (2007) 403–423.
[13] T.M. Wang, R.H. Nettleton, B. Keita, Natural frequencies for out-of-plane vibrations of continuous curved beams, *Journal of Sound and Vibration* 68 (1980) 427–436.
[14] J.M. Snyder, J.F. Wilson, Free vibrations of continuous horizontally curved beams, *Journal of Sound and Vibration* 157 (1992) 345–355.
[15] M.T. Piovan, V.H. Cortinez, R.E. Rossi, Out-of-plane vibrations of shear deformable continuous horizontally curved thin-walled beams, *Journal of Sound and Vibration* 237 (2000) 101–118.
[16] T.M. Wang, W.F. Brannen, Natural frequencies of out-of-plane vibrations of curved beams on elastic foundations, *Journal of Sound and Vibration* 84 (1982) 241–246.
[17] M.S. Issa, M.E. Nasr, M.A. Naiem, Free vibrations of curved Timoshenko beams on Pasternak foundations, *International Journal of Solids and Structures* 26 (1990) 1243–1252.
[18] B.K. Lee, S.J. Oh, K.K. Park, Free vibrations of shear deformable circular curved beams resting on an elastic foundation, *International Journal of Structural Stability and Dynamics* 2 (2002) 77–97.
[19] S.P. Timoshenko, On the correction for shear of the differential equation for transverse vibrations of prismatic bars, *Philosophical Magazine* 41 (1921) 744–746.
[20] E. Volterra, J.H. Gaines, *Advanced Strength of Materials*, Prentice-Hall, Englewood Cliffs, NJ, 1971.
[21] B.K. Lee, J.F. Wilson, Free vibrations of arches with variable curvature, *Journal of Sound and Vibration* 136 (1990) 75–89.
[22] B. Carnahan, H.A. Luther, J.O. Wilkes, *Applied Numerical Methods*, Wiley, New York, 1969.
[23] S.P. Timoshenko, J.N. Goodier, *Theory of Elasticity*, McGraw-Hill, New York, 1970.
[24] D.J. Ewins, *Modal Testing: Theory, Practice and Application*, Research Studies Press, Philadelphia, 2000.